Supporting information for

Oxygen Vacancy Induced Efficient Hydrogen Spillover of $Ni_{17}W_3/WO_{3-x}/MoO_{3-x}$ for Superior pH-Universal Hydrogen Evolution Reaction

Yiqing Sun[a,b], Yiwei Bao[a,b], Di Yin[c], Xiuming Bu[b*], Yuxuan Zhang[c], Kaihang Yue[b], Xiaoshuang Qi[b], Ziyan Cai[b], Yongqiang Li[d], Xiulan Hu[a*], Johnny C. Ho[c,e*], Xianying Wang[b*]

[a] College of Materials Science and Engineering, Nanjing Tech University, Puzhu South Road No.30, 211816, Nanjing, Jiangsu, China

[b] CAS Key Laboratory of Materials for Energy Conversion, Shanghai Institute of Ceramics, Chinese Academy of Sciences, Shanghai 200050, P. R. China

[c] Department of Materials Science and Engineering City University of Hong Kong Kowloon, Hong Kong SAR 999077, P. R. China

[d] Joint Laboratory of Graphene Materials and Applications, Shanghai Institute of Microsystem and Information Technology, Chinese Academy of Sciences, Shanghai 200050, P. R. China

[e] Institute for Materials Chemistry and Engineering, Kyushu University, Fukuoka 816–8580, Japan

*Corresponding author. E-mail: buxiuming@mail.sic.ac.cn (Xiuming Bu); whoxiulan@163.com (Xiulan Hu); johnnyho@cityu.edu.hk (Johnny C. Ho); wangxianying@mail.sic.ac.cn (Xianying Wang)

Supplementary Figures and Tables

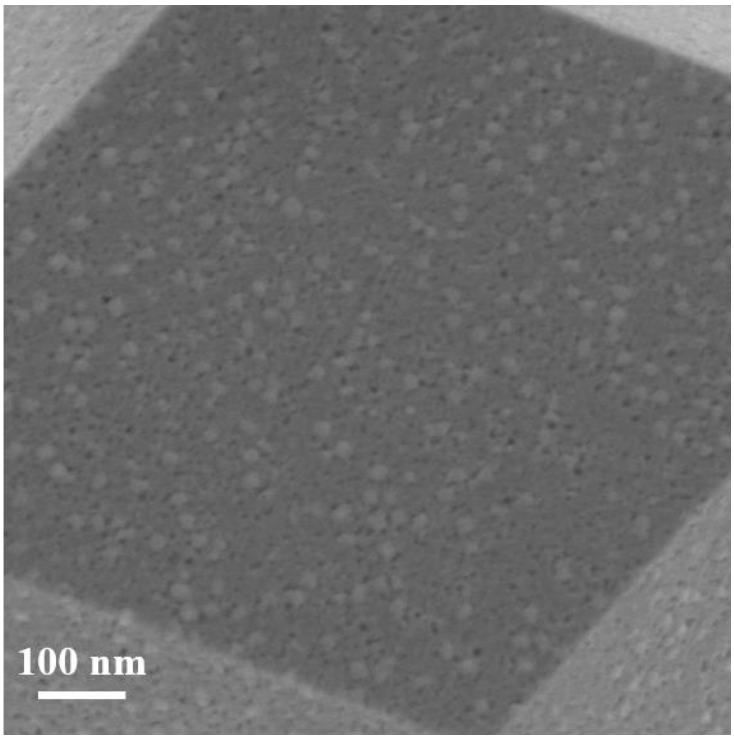

Figure S1. High-magnification SEM image of the NWP.

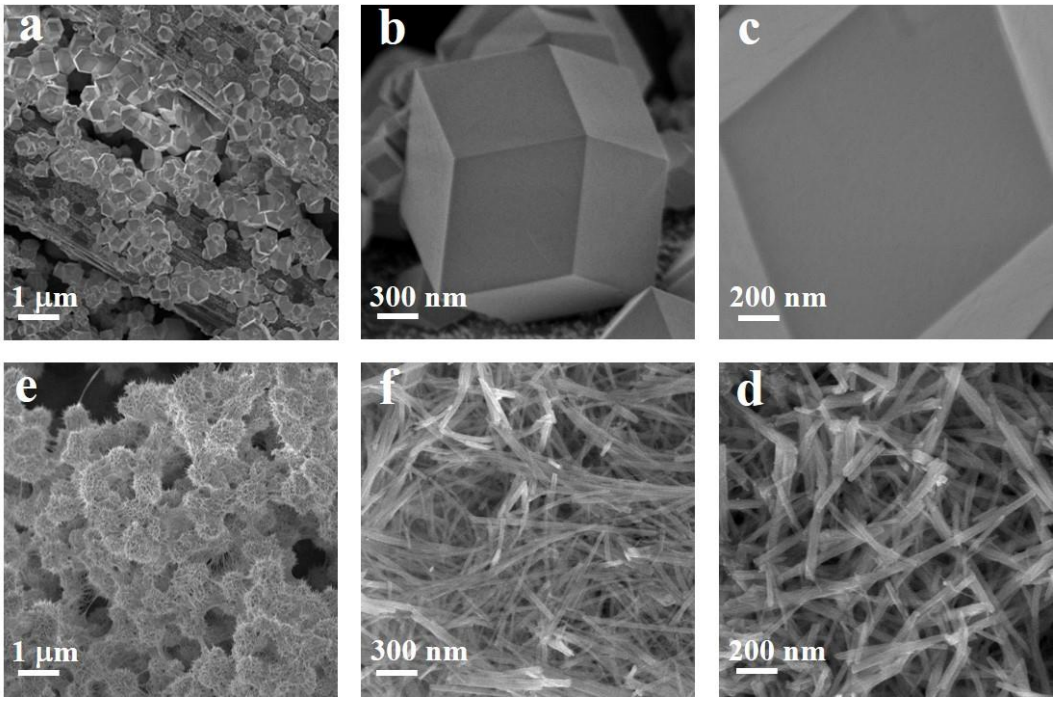

Figure S2. Low- and high-magnification SEM images of (a-c) $Ni_4W_6O_{21}$, (e-d) Mo-$Ni_4W_6O_{21}$.

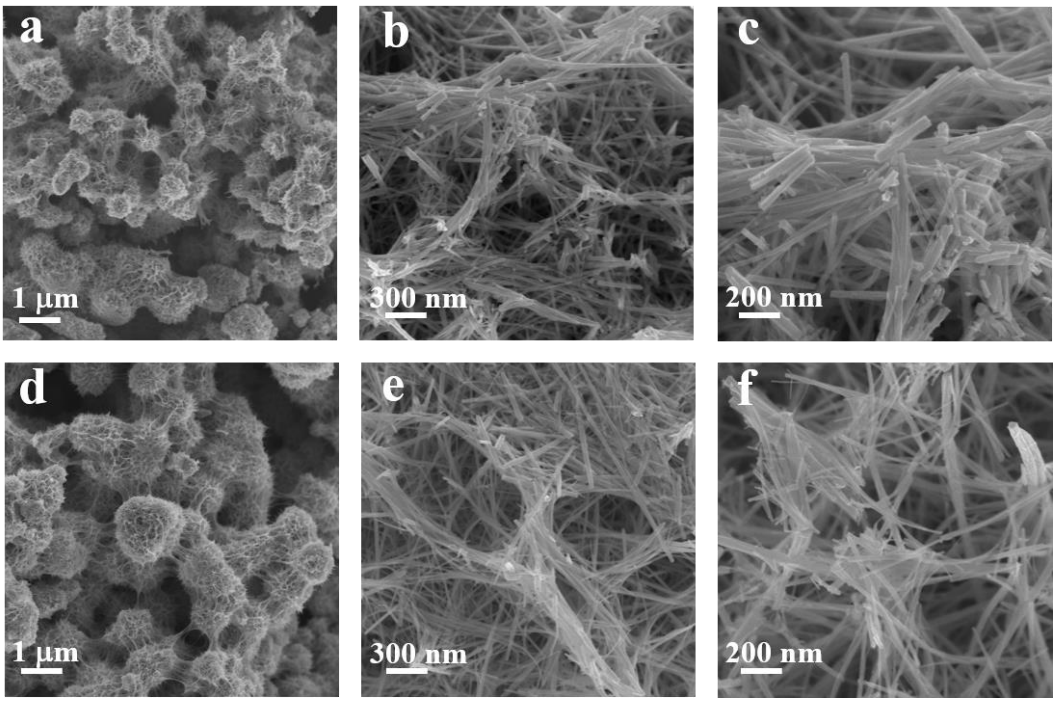

Figure S3. Low- and high-magnification SEM images of (a-c) $NiW_1M_{0.5}R$, (e-d) $NiW_1M_{1.5}R$.

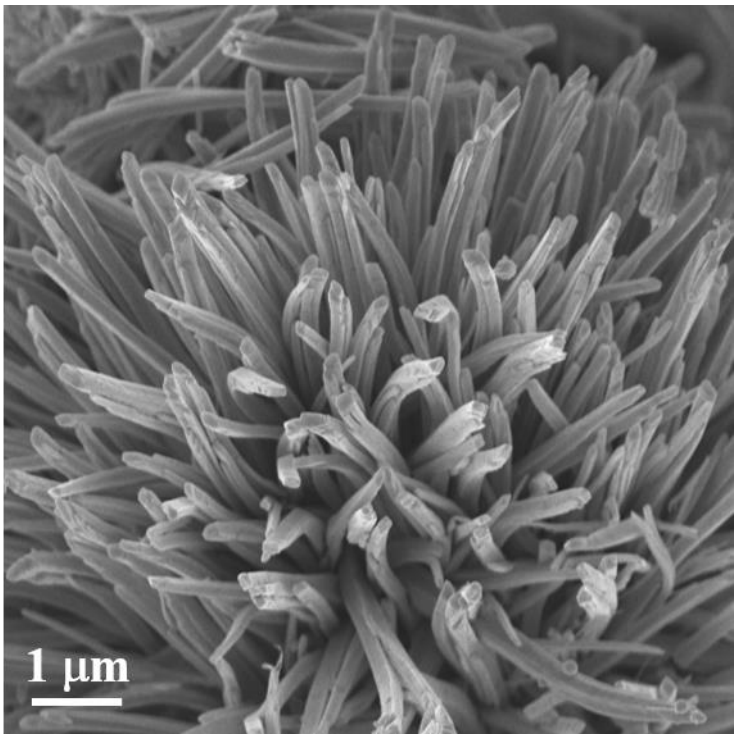

Figure S4. SEM images of the NMR.

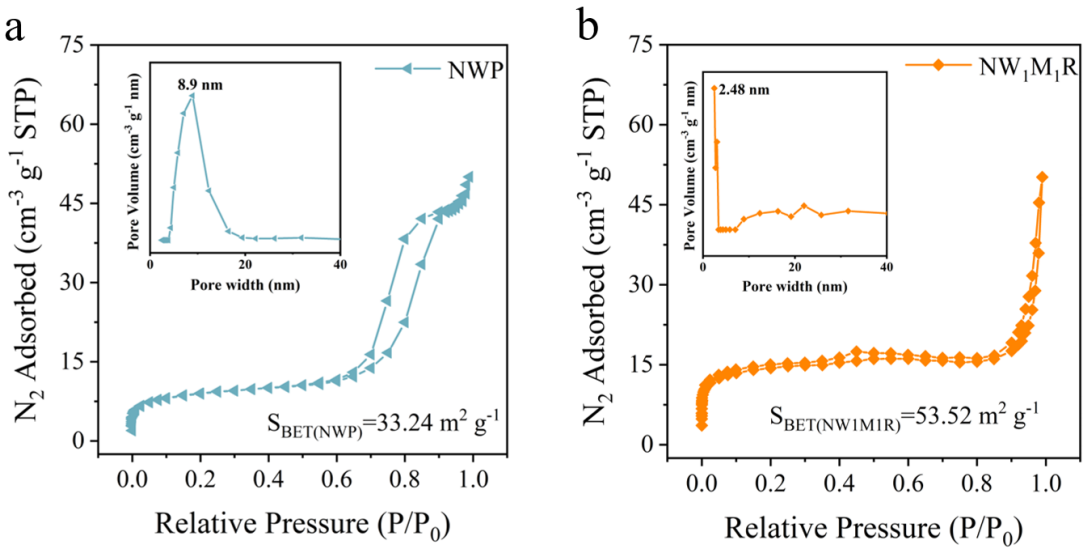

Figure S5. Argon adsorption and desorption isotherms of NWP (a) and NW_1M_1R (b), the inset shows the corresponding pore size distribution curve.

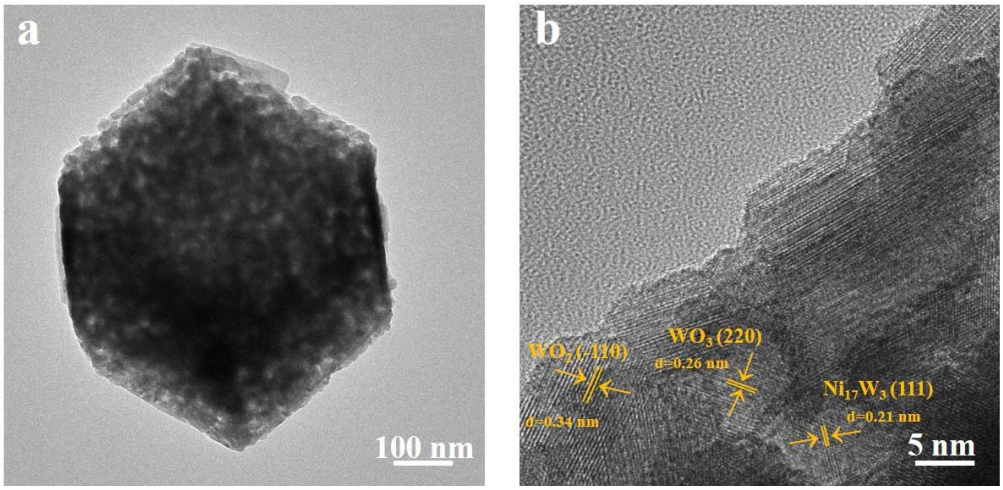

Figure S6. (a) TEM and (b) HRTEM images of NWP.

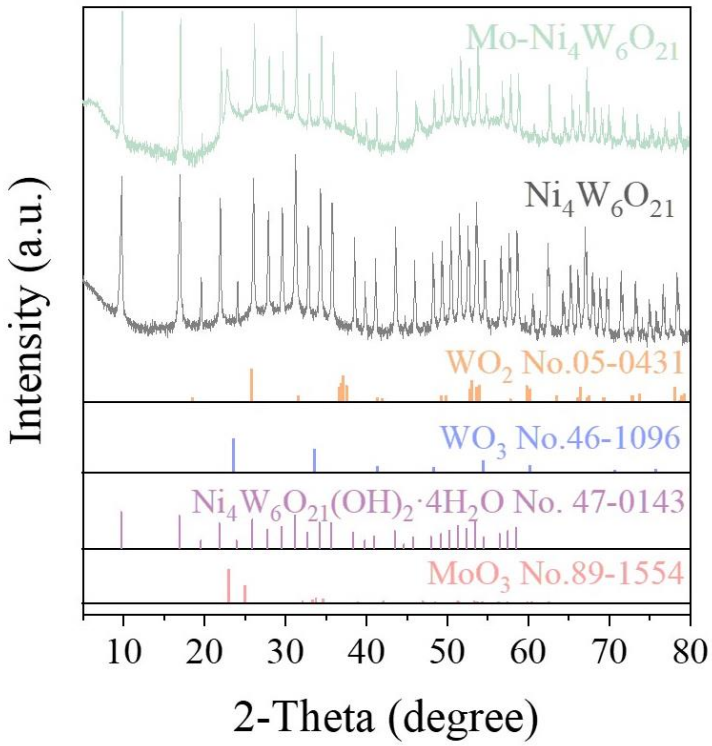

Figure S7. XRD patterns of the Mo-$Ni_4W_6O_{21}$ and $Ni_4W_6O_{21}$.

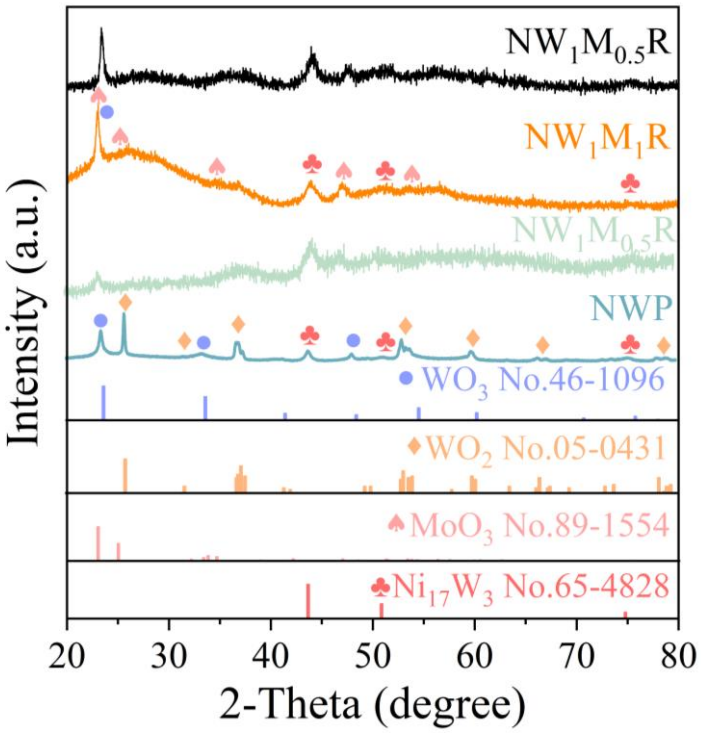

Figure S8. XRD patterns of the $NiW_1M_{0.5}R$, NW_1M_1R, $NiW_1M_{1.5}R$ and NWP.

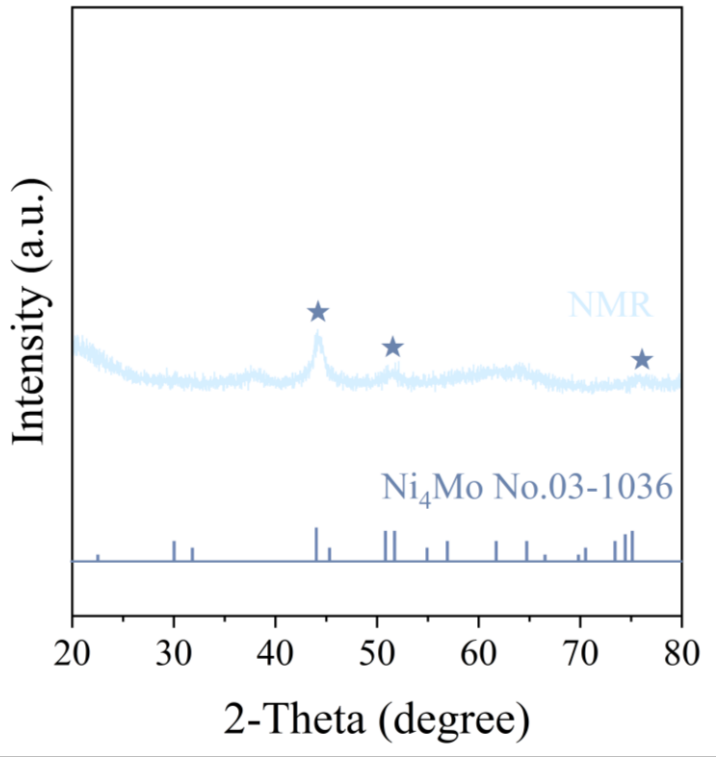

Figure S9. XRD patterns of the NMR.

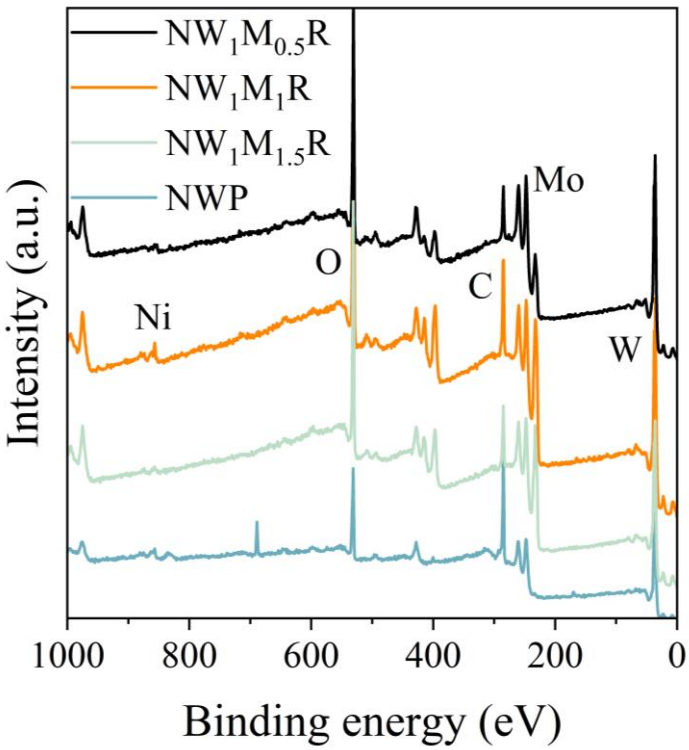

Figure S10. Full XPS spectrum of $NW_1M_{0.5}R$, NW_1M_1R, $NW_1M_{1.5}R$, snd NWP.

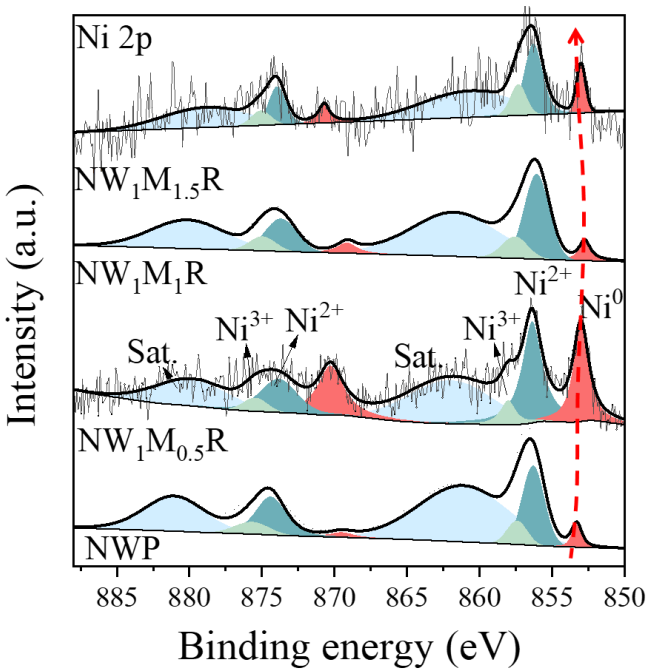

Figure 11. High-resolution XPS signals of Ni 2p for $NW_1M_{0.5}R$, $NW_1M_{1.5}R$, NW_1M_1R and NWP.

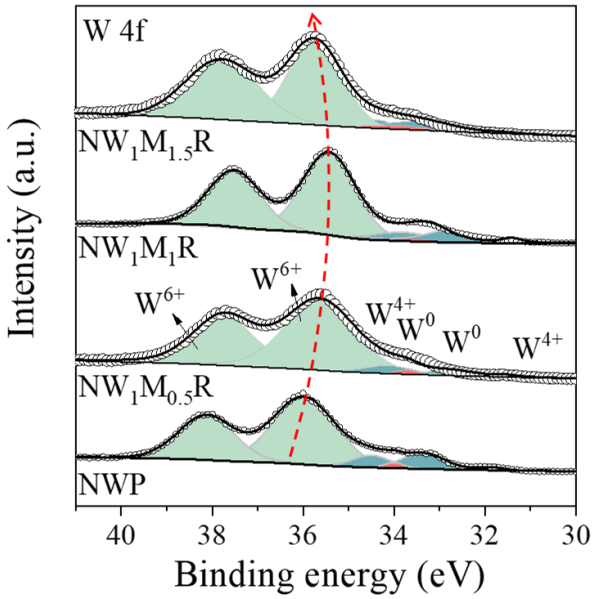

Figure S12. High-resolution XPS signals of W 4f for $NW_1M_{0.5}R$, $NW_1M_{1.5}R$, NW_1M_1R and NWP.

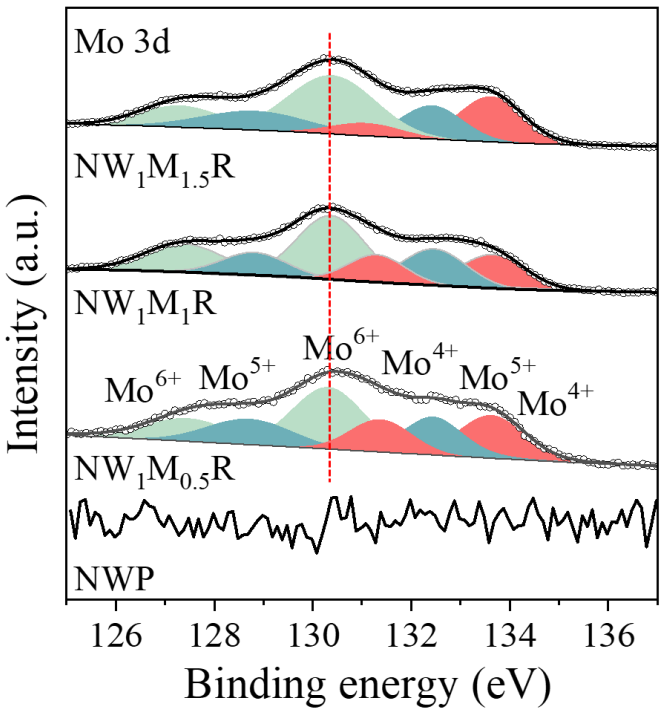

Figure S13. High-resolution XPS signals of Mo 3d for $NW_1M_{0.5}R$, $NW_1M_{1.5}R$, NW_1M_1R and NWP.

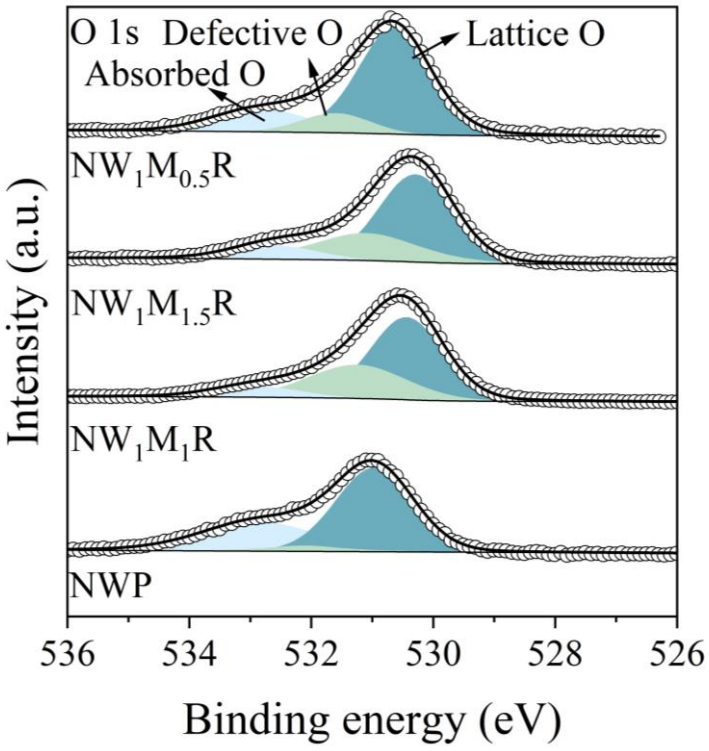

Figure S14. High-resolution XPS signals of O 1s for $NW_1M_{0.5}R$, $NW_1M_{1.5}R$, NW_1M_1R, and NWP.

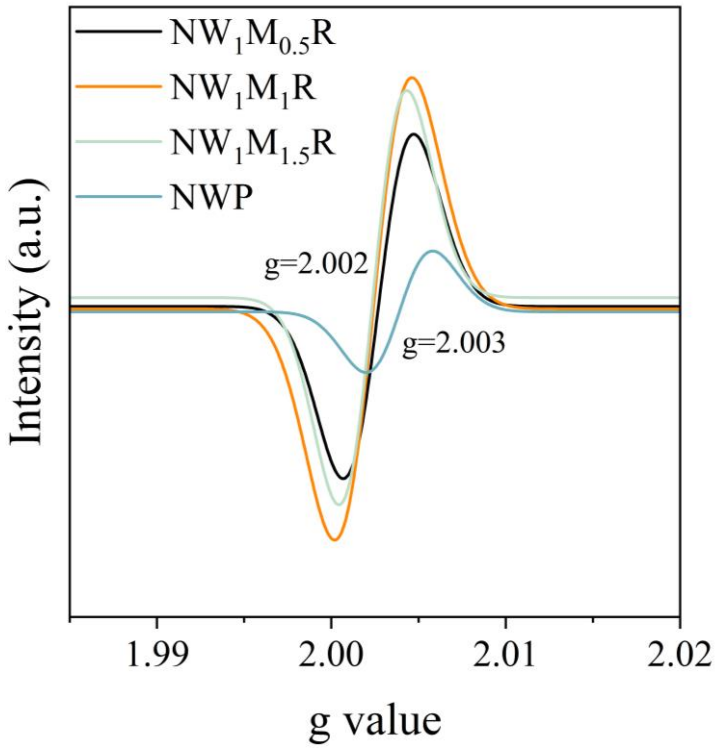

Figure S15. EPR spectra of $NW_1M_{0.5}R$, NW_1M_1R, $NW_1M_{1.5}R$ and NWP.

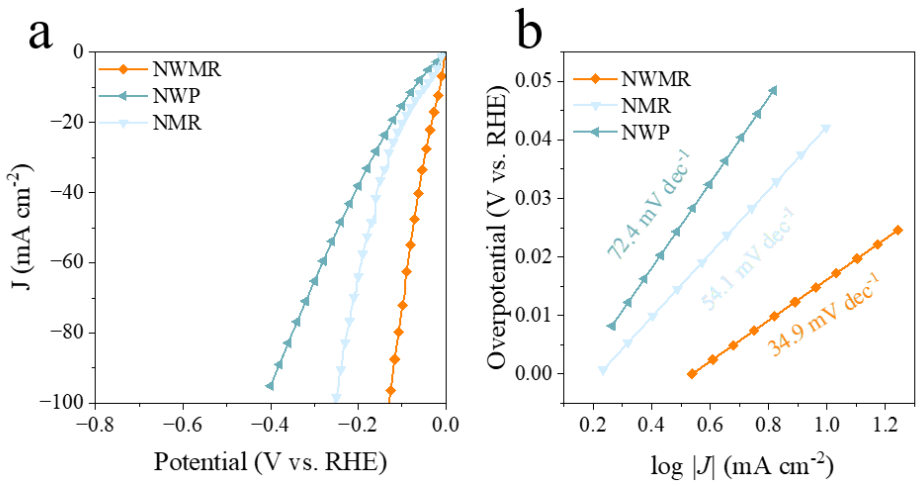

Figure S16. (a) LSV curves of NW_1M_1R, NMR, and NWP and (b) Tafel slope of different electrodes.

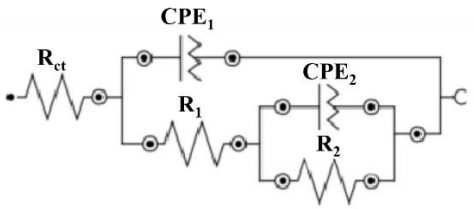

Figure S17. Equivalent circuit diagram of $NW_1M_{0.5}R$, NW_1M_1R, $NW_1M_{1.5}R$ and NWP.

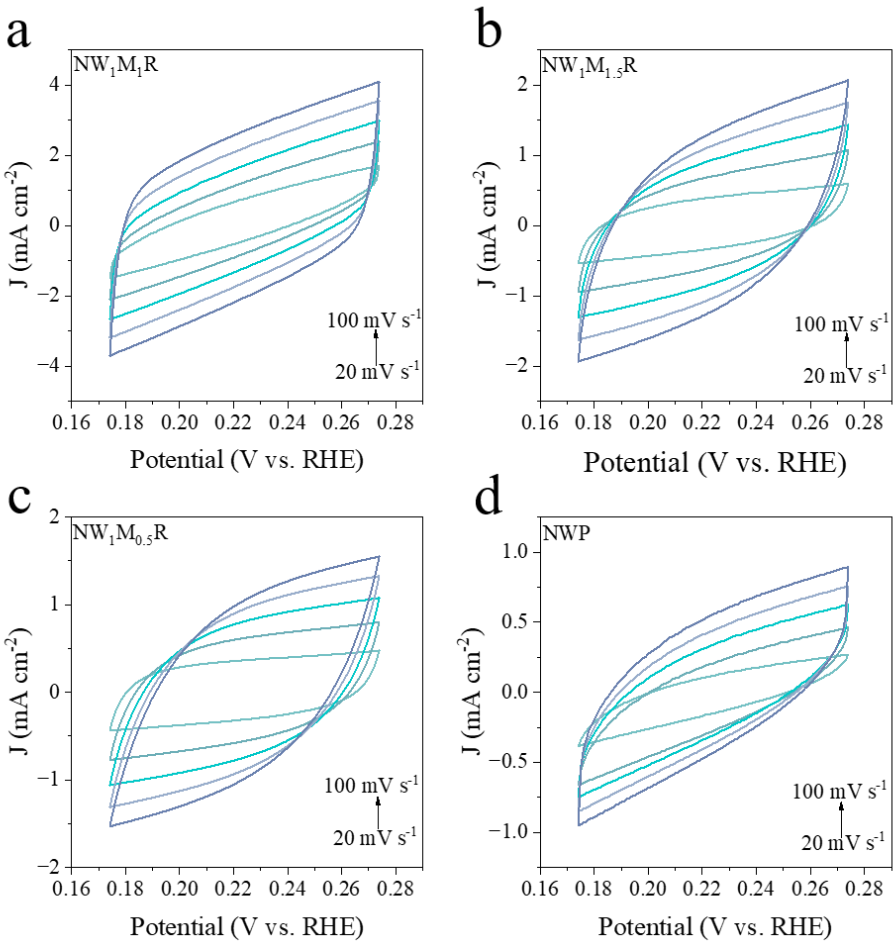

Figure S18. CV curves at different scan rates ranging from 20 mV s^{-1} to 100 mV s^{-1} (a) NW_1M_1R, (b) $NW_1M_{1.5}R$, (c) $NW_1M_{0.5}R$, and (d) NWP. The potential scanning rates are from 0.173 V to 0.273 V vs. RHE with an interval of 20 mV s^{-1}.

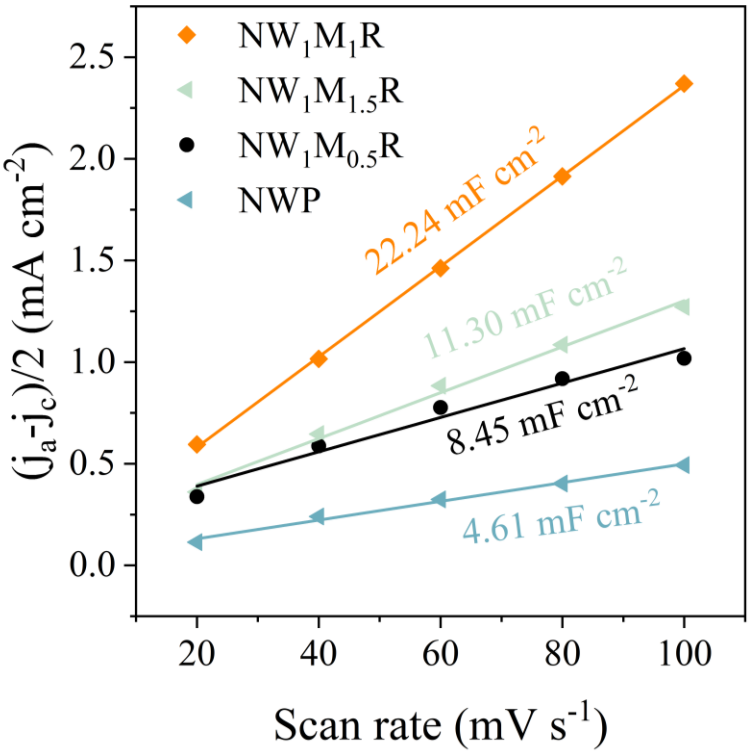

Figure S19. C_{dl} of NW_1M_1R, $NW_1M_{1.5}R$, $NW_1M_{0.5}R$ and NWP.

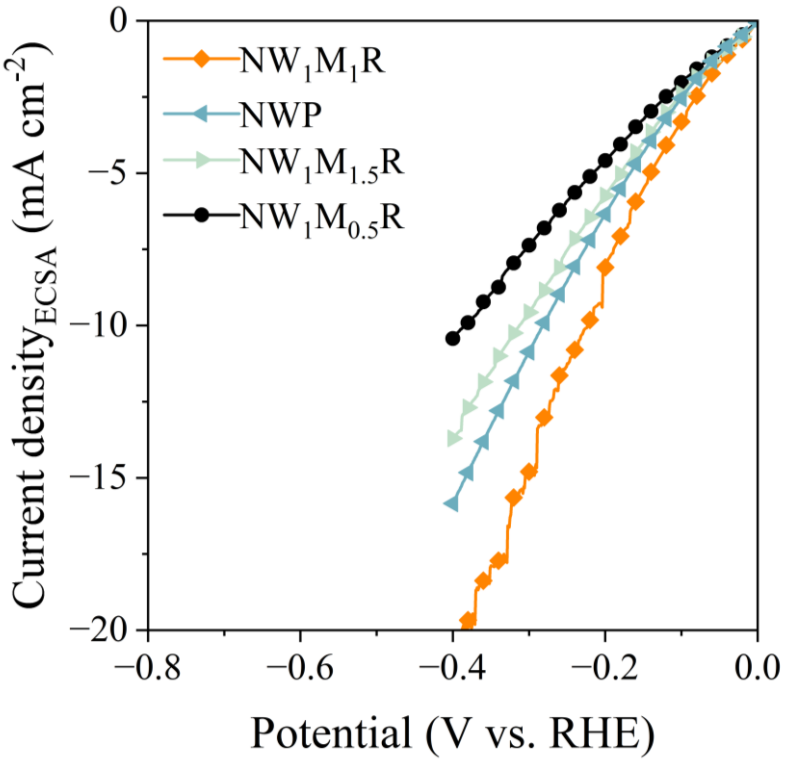

Figure S20. ECSA-normalized LSV of the NW_1M_1R, $NW_1M_{1.5}R$, $NW_1M_{0.5}R$, and NWP**.**

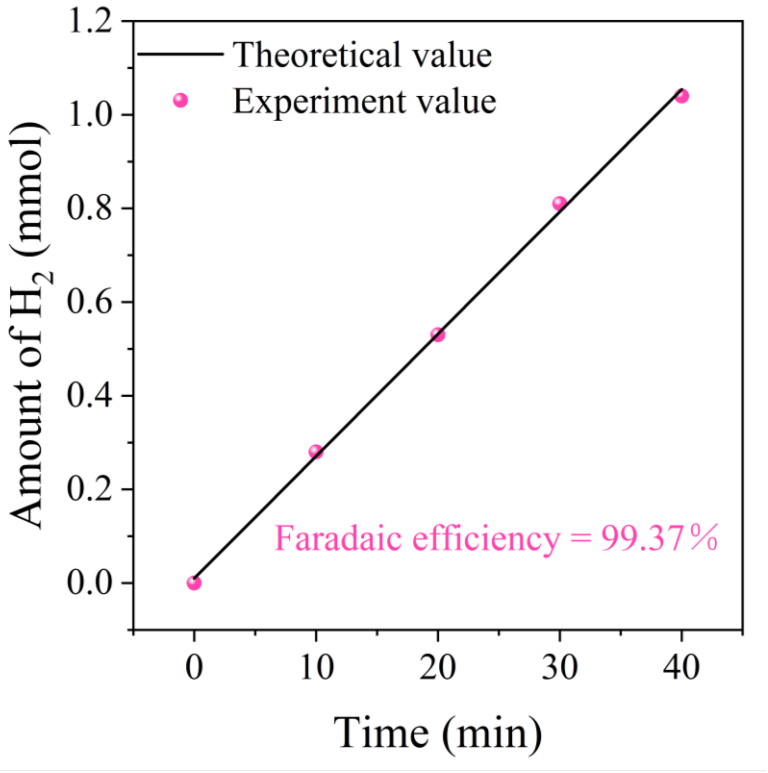

Figure S21. Faradic efficiency measurements.

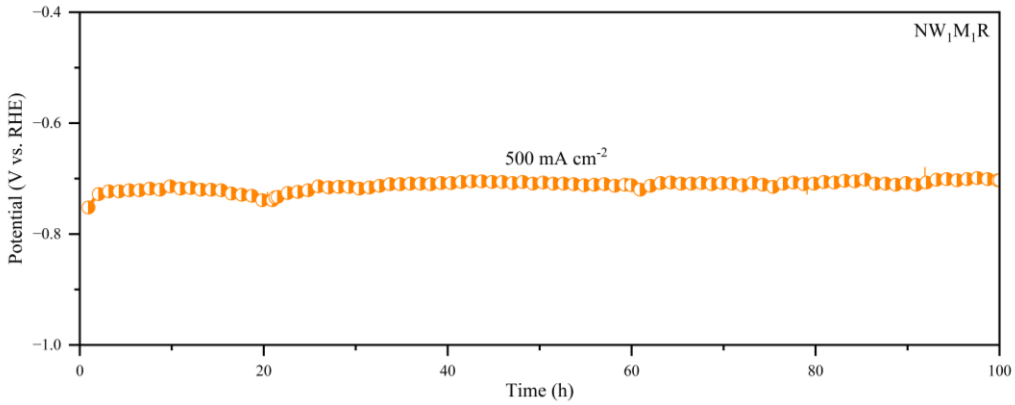

Figure S22. Chronopotentiometry stability tests of the NW_1M_1R electrodes under the high current density of 500 mA cm^{-2} (without iR correction).

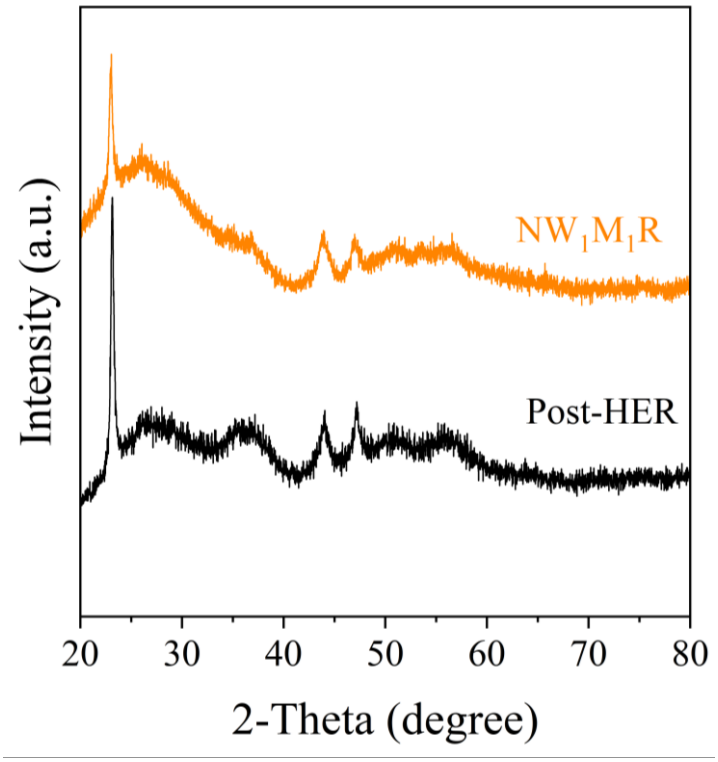

Figure R23. XRD patterns of NW_1M_1R and Post- HER.

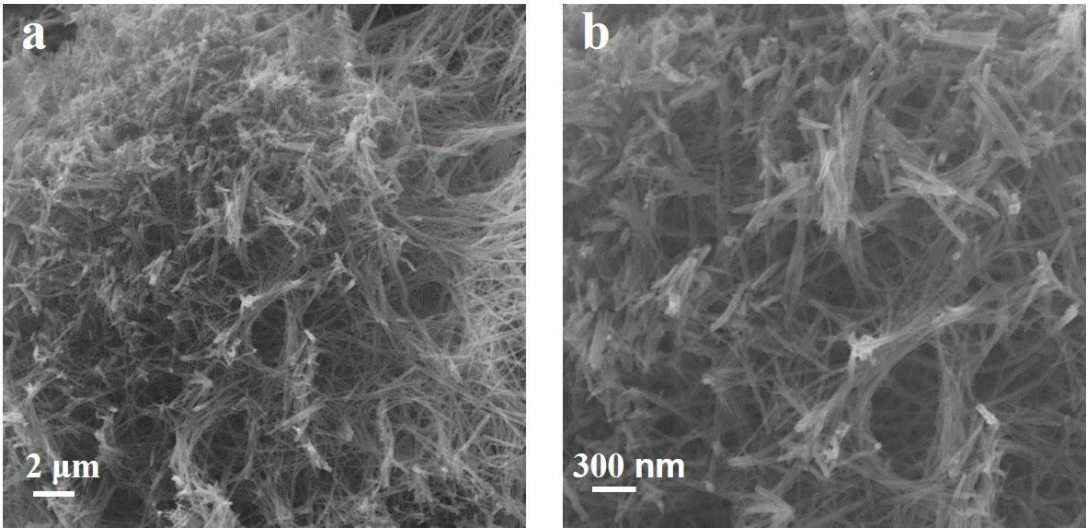

Figure S24. SEM image of NW_1M_1R after HER stabilization for 160 h at 1.0 M KOH.

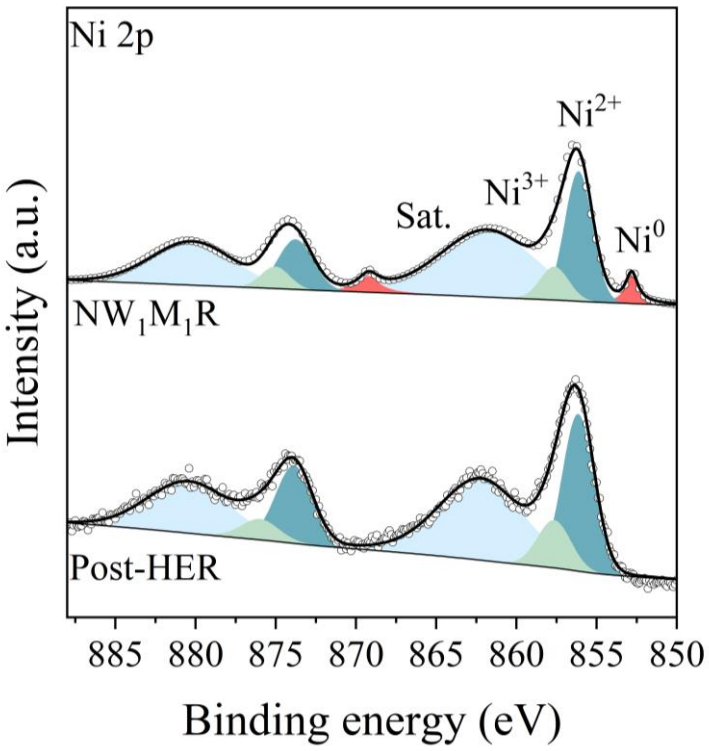

Figure S25. High-resolution XPS signals of Ni 2p for NW_1M_1R and Post- HER.

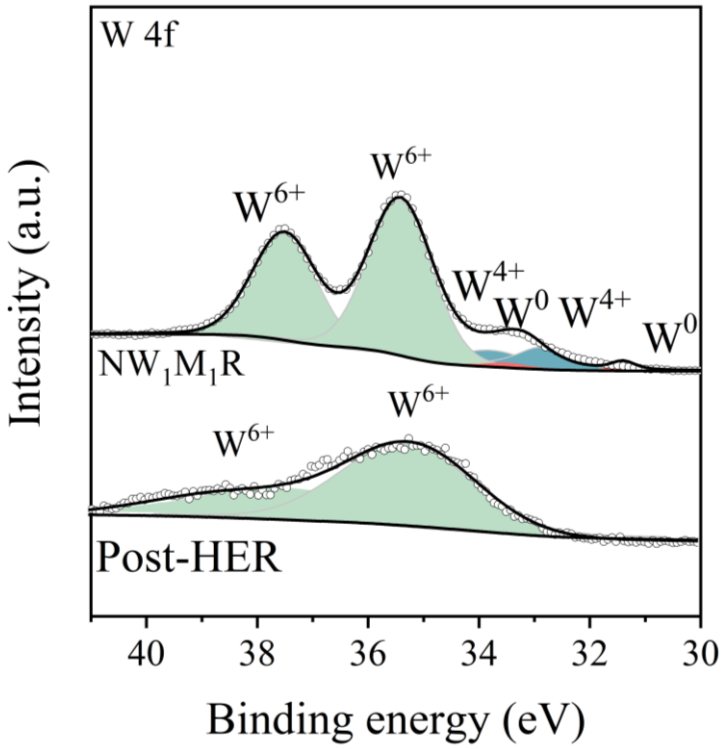

Figure S26. High-resolution XPS signals of W 4f for NW_1M_1R and Post- HER.

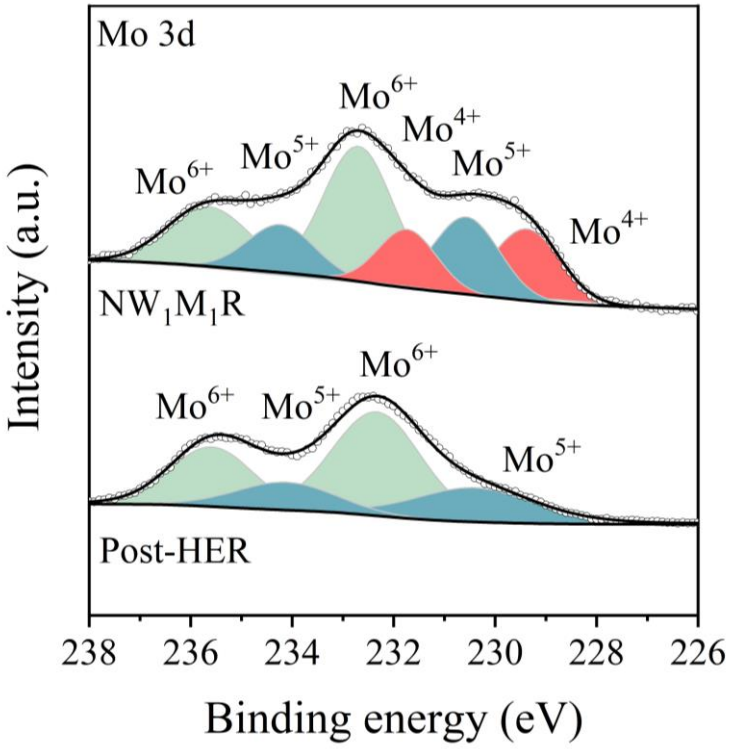

Figure S27. High-resolution XPS signals of Mo 3d for NW_1M_1R and Post- HER.

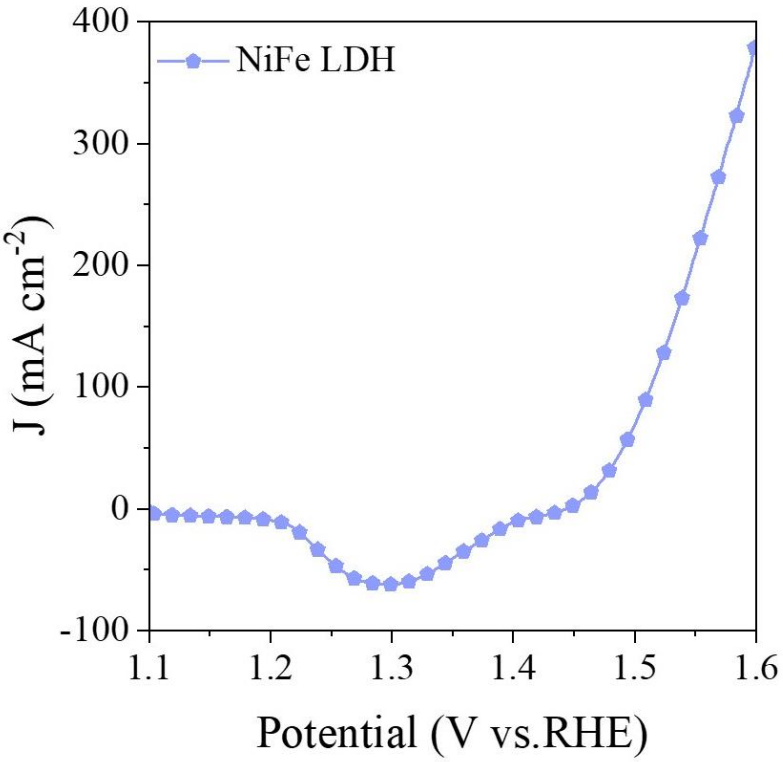

Figure S28. LSV curves of home-made NiFe LDH in 1.0 M KOH.

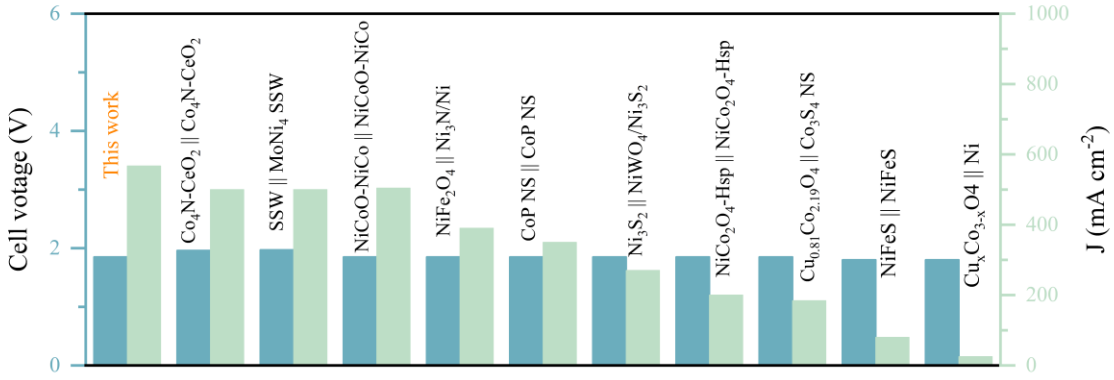

Figure S29. AEM performance comparison with NW_1M_1R and recently reported electrocatalyst.

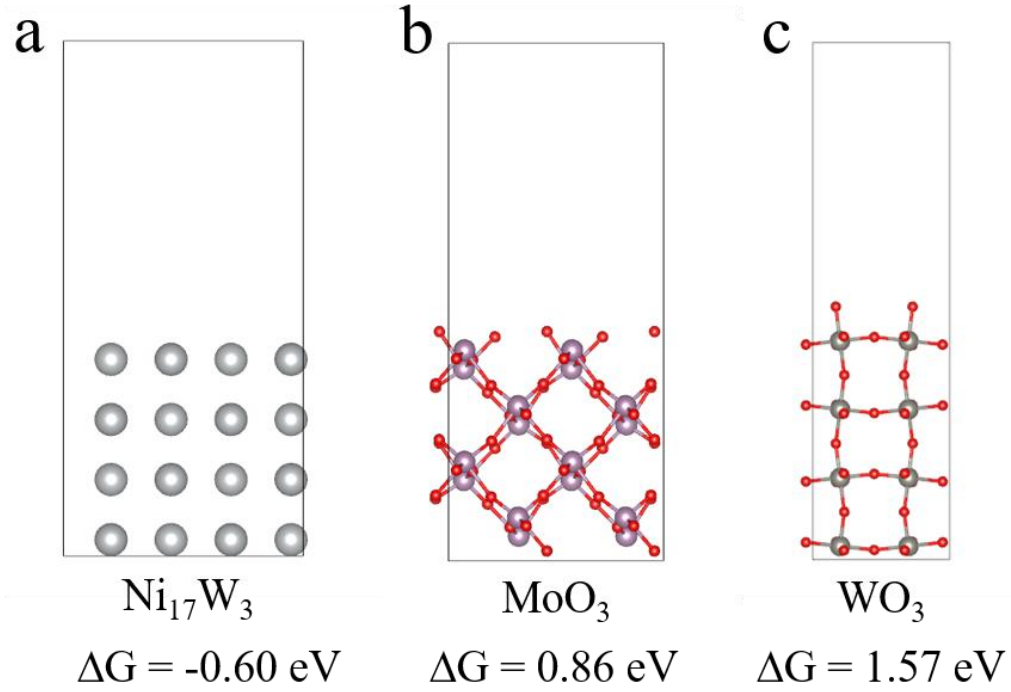

Figure S30. ΔG of $Ni_{17}W_3$, MoO_3 and WO_3.

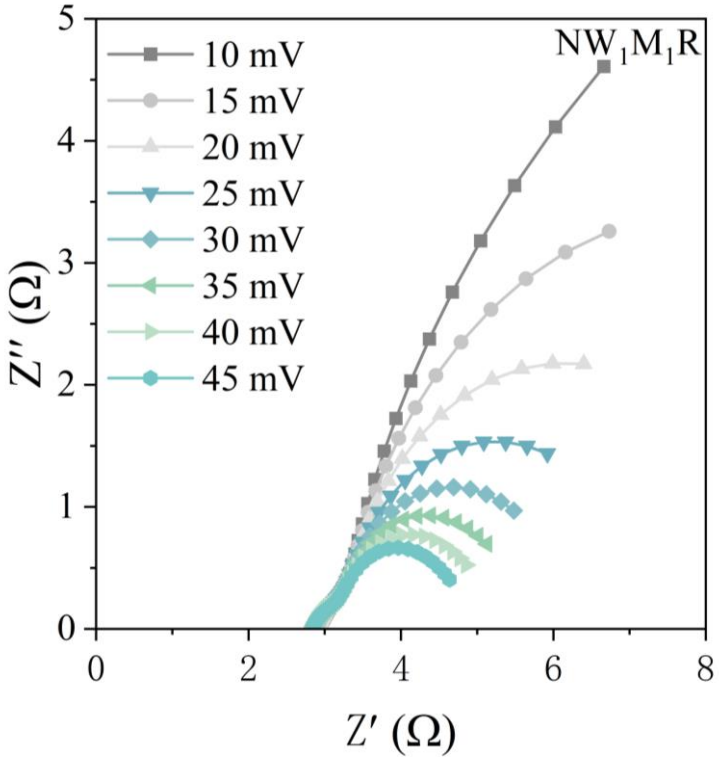

Figure S31. Nyquist plots of NW_1M_1R in 1.0 M KOH at various HER overpotentials.

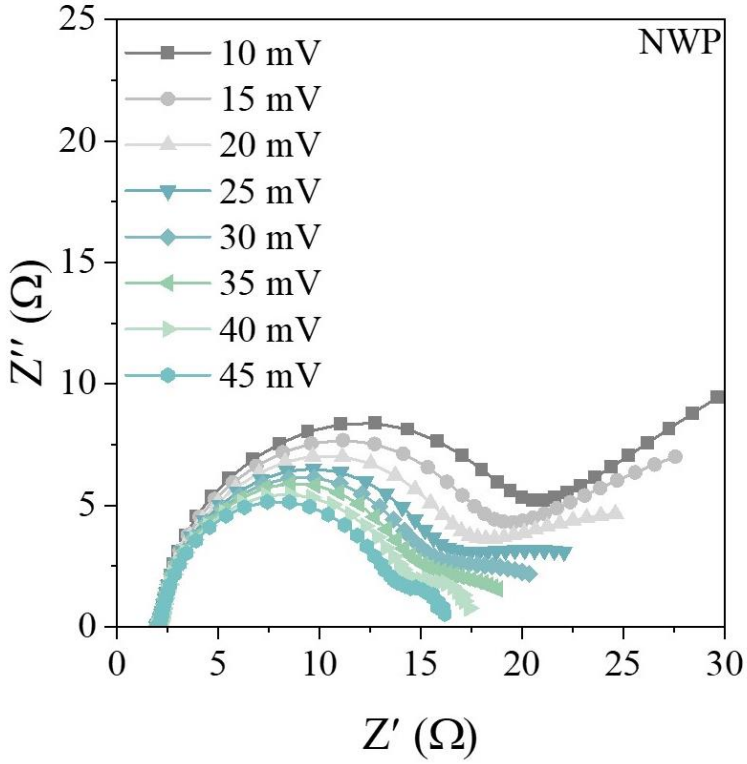

Figure S32. Nyquist plots of NWP in 1.0 M KOH at various HER overpotentials.

Table S1. Comparisons of the HER catalytic activity of hierarchical NW_1M_1R electrode in 1.0 M KOH electrolyte with representative electrocatalysts reported previously.

Electrocatalyst	Overpotentials (mV) at 10 mA cm^{-2}	Tafel slope (mV dec^{-1})	Reference
NW_1M_1R	**16**	**34.9**	**This work**
WC-N/W	87	44.9	*Adv. Sci.* **2022**, 9, 2106
NiMo/$Co(OH)_2$@CC	30	41	*Adv. Funct. Mater.* **2021**, *31*, 2102117
NiMo/Ni-P	32	60.85	*Nat. Commun.* **2018**, *9*, 2014
MoO_3/Ni-NiO	62	59	*Adv. Mater.* **2020**, *32*, 2003414
β-$NiMoO_4$	23	44	*Nat. Commun.* **2021**, *12*, 5960.
$NiMoO_x$/NiMoS	38	38	*Nat. Commun.* **2020**, *11*, 5462
MoS_2/Co_9S_8/Ni_3S_2/Ni	113	85	*J. Am. Chem. Soc.* **2019**, *141*, 10417
$IrMo_{0.59}$ NPs	23	50	*Adv. Mater.* **2020**, *32*, 2006034.
DS IrNi@CNTS	17	48	*ACS Catal.* **2020**, *10*, 7322-7327
Co/MoN	52	77.5	*Appl. Catal. B* **2021**, *286*, 119882
Ni_2P/MoS_2	149	60.2	*Adv. Funct. Mater.* **2019**, *29*, 1809151
Ni_3N-NiMoN	31	64	*Nano Energy* **2018**, *44*, 353-363
FeP/Ti	97	64	*Appl. Catal. B* **2020**, *260*, 118156
P-MoP/Mo_2N	89	78	*Angew. Chem. Int. Ed.* **2021**, *60*, 6673-6681

Table S2. The fitted parameters of the EIS data of NWP catalysts for HER.

Catalyst	η (mV)	R_s (Ω)	CPE_1-T	CPE_1-P	R_1 (Ω)	CPE_2-T	CPE_2-P	R_2(Ω)
	10	2.046	0.008685	0.89501	19.22	0.37296	0.72155	32.77
	15	2.056	0.008624	0.89624	17.64	0.48110	0.76287	18.50
	20	2.069	0.008486	0.89514	16.25	0.60179	0.80656	11.04
NWP	25	2.059	0.008393	0.89588	15.04	0.73284	0.85480	7.063
	30	2.068	0.008333	0.89522	14.23	0.85369	0.89342	5.069
	35	2.073	0.008211	0.89666	13.61	1.11300	0.98337	3.452
	40	2.059	0.008294	0.89383	12.84	1.31100	0.98950	2.657
	45	2.060	0.008199	0.89546	12.05	1.4480	0.99870	2.153

Table S3. The fitted parameters of the EIS data of NW_1M_1R catalysts for HER.

Catalyst	η (mV)	R_s (Ω)	CPE_1-T	CPE_1-P	R_1 (Ω)	CPE_2-T	CPE_2-P	R_2(Ω)
	10	3.035	0.74778	0.83254	1.163	0.7300	0.82853	14.22
	15	3.021	0.74539	0.84010	1.078	0.8764	0.85580	7.568
	20	3.039	0.83357	0.86548	1.218	1.1190	0.89389	4.336
NW_1M_1R	25	3.022	0.80187	0.85017	1.068	1.2940	0.90824	2.957
	30	3.000	0.76032	0.86896	0.895	1.4260	0.90796	2.208
	35	2.998	0.77300	0.85863	0.834	1.6610	0.91558	1.662
	40	2.991	0.76607	0.86803	0.793	1.8250	0.92734	1.311
	45	2.982	0.75020	0.85792	0.706	1.9600	0.92208	1.111